Discharge Pattern Discrimination in Vacuum Interrupter with Non-contact Measurement of Shield Potential

Fei Kong, Hiroki Kojima, Naoki Hayakawa
Department of Electrical Engineering and Computer Science, Nagoya University
Furo-cho, Chikusa-ku, Nagoya, 464-8603, Japan

Toshinori Kimura and **Mitsuru Tsukima**
Mitsubishi Electric Corporation
Advanced Technology R&D Center
8-1-1, Tsukaguchi-honmachi, Amagasaki, 661-8661, Japan

ABSTRACT

Vacuum interrupter has a composite insulation system. When an internal insulation fails, the discharge has complex and various patterns. Previously, based on the discharge development characteristics, we proposed a discrimination method for the discharge pattern in vacuum interrupter. We measured the applied voltage, anode current, and shield potential waveforms, respectively. From the analysis of the measured waveforms, we can estimate the discharge patterns and discharge path lengths. In this paper, a non-contact shield potential measurement was proposed when the shield potential cannot be measured directly. Furthermore, verification tests with this measurement method were conducted and the effectiveness of the discrimination method was confirmed.

  Index Terms — **Vacuum interrupter, floating electrode, discharge diagnostics, breakdown, surface flashover**

1 INTRODUCTION

  SINCE 1980s, vacuum circuit breakers (VCB) have been utilized worldwide in medium voltage system and distribution power networks [1]. The internal insulation problem of vacuum interrupters (VI) constrains the development of VCBs in the higher voltage systems [2-3]. Because VI has a composite insulation system, the discharge in VI has complex patterns for various discharge sites and paths. The discharge mainly occurs at insulation weakness points which may exist in VI, such as breakdown (BD) between vacuum gaps, surface flashover (FO) on insulator, and the combination patterns with BD and FO, as shown in Figure 1. Therefore, the discharge discrimination is significant for the efficient and reliable insulation design of VCB.

  Previously, based on discharge development characteristics, we proposed a novel discrimination method of the discharge pattern in VI [4-5]. In this method, shield potential is a key factor for determining whether the discharge passed through the shield or not. However, it is not always possible to measure the shield potential directly in VI. Therefore, a new shield potential measurement method is necessary.

  In this paper, we focus on the discharge discrimination with non-contact shield potential measurement method. An electrostatic probe was set on the outside of insulator of VI.
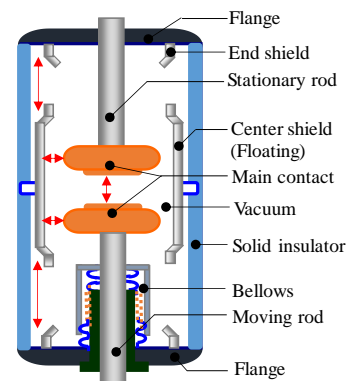
Figure 1. Possible discharge pattern in VI (red arrows represent possible discharge paths)

The shield potential can be calculated from the measured value by the electrostatic probe. Correspondingly, the discharge pattern discrimination method with the electrostatic probe was proposed and its effectiveness was verified.

2 DISCHARGE PATTERN DISCRIMINNATION METHOD

  By the measurement of electrical parameters (applied voltage, anode current, shield potential), we picked up the discharge features for each discharge pattern, respectively, and we proposed a discrimination flowchart as shown in Figure 2 which consisted of 3 steps [4-5]:

STEP 1: By the analysis of the features of applied voltage, anode current, and shield potential waveforms, we determine whether the discharge passed through the shield or not.

STEP 2: Based on the relation between the discharge development time and path length in the fundamental discharge characteristics from our database as shown in Figure 3, we estimate the possible discharge patterns and path lengths.

STEP 3: We discriminate the discharge site (insulation weakness) in consideration of the internal structure and dimension of VI.

The discharge mechanism in Figure 3 can be explained as follows: For the BD process in vacuum gap, according to the cathode plasma expansion model [6-8], the cathode plasma can be produced at the cathode surface and expand to the anode. The cathode plasma expansion velocity was calculated to be in the order of 10^4 m/s, which was determined by the electrode material, and independent of the potential difference between the cathode and the shield, i.e. electric field strength. BD development time T_{BD} depends on the gap length g monotonically, therefore, we can estimate the gap length from

the measurement of T_{BD} [9-10]. For the FO process on insulator, the discharge starts with the explosive electron emission on cathode surface. According to the electron-stimulated outgassing model [11-13], FO development time T_{FO} is proportional to V_{FO}^{-2} and T_{FO} increased with increasing surface distance d for a certain V_{FO} [9-10]. Based on the relation between T_{FO} and d, the surface distance can be estimated from the measurement of T_{FO} and V_{FO}. The discrimination success rate with the above method reached as high as 93% [4].

3 DISCRIMINATION METHOD WITH ELECTROSTATIC PROBE

3.1 VI MODEL

Figure 4 shows the VI model for the discrimination of discharge pattern. The VI model consisted of upper electrode (u), cathode (c), anode (a), lower electrode (l), shield (s) and insulator (i), which can simulate the actual internal structure of VI. The upper and lower electrodes had plane shape and were made of stainless steel. The cathode and the anode had plane shape and were made of copper. The cathode and the anode were connected with the upper electrode and the lower electrode, respectively. The floating electrode as a shield was placed on the center of insulator. The shield was made of stainless steel with the dimension of 120 mm × 60 mm × 2 mm. The insulator was alumina ceramic (Al_2O_3, purity: 92%) with the dimension of 150 mm × 150 mm × 5 mm. The upper and lower electrodes were contacted with the insulator.
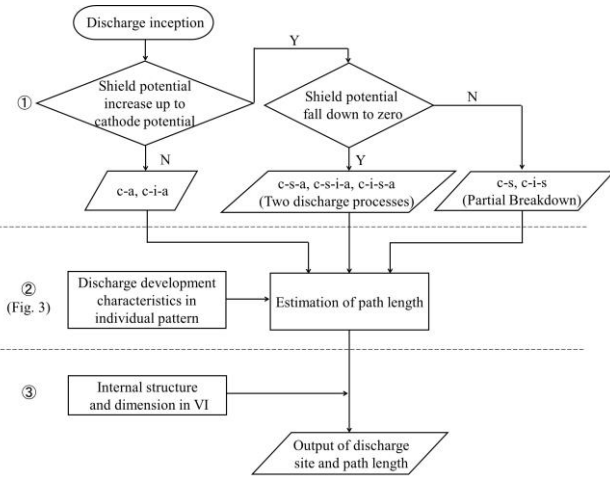

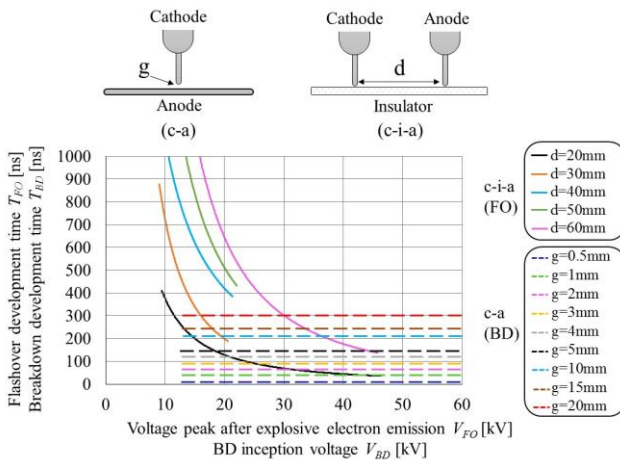**Figure 2.** Discrimination flowchart

Figure 3. Fundamental discharge development characteristics for BD and FO
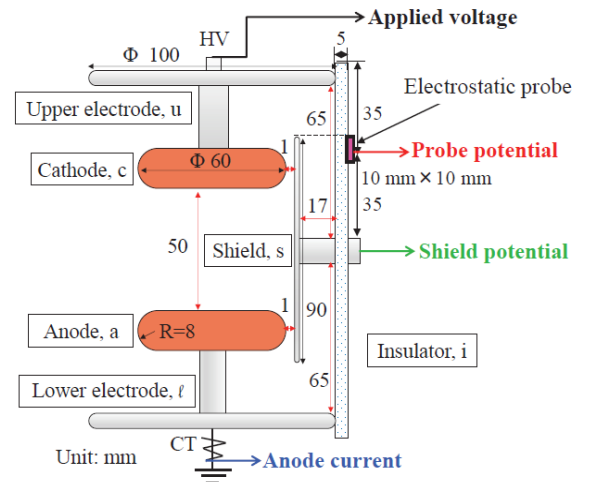

Figure 4. VI model with an electrostatic probe.

We measured the applied voltage waveform with a voltage divider (1/45900), the anode current with a high frequency current transformer (1-20 MHz). A metal sheet with the dimension of 10 mm × 10 mm as an electrostatic probe was set on outside of the insulator behind the shield to measure the shield potential indirectly. At the same time, the shield potential was measured by a high voltage probe (input impedance: 100 MΩ) directly. The VI model was set in a vacuum chamber with 10^{-5} Pa. The impulse generator

provided a negative standard lightning impulse voltage (1.2/50 μs). These waveforms were acquired by a digital oscilloscope (2.5 GHz, 40 GS/s). In addition, still images of discharge were captured with a digital camera to check the discharge patterns.

3.2 SHIELD POTENTIAL DETERMINATION

Figure 5 shows discharge waveforms and light emission for a discharge through cathode-shield-anode (c-s-a) at the applied voltage $V_a=-43$ kV$_{peak}$. The discharge process is as follows: Firstly, the discharge between cathode and shield occurred (V_1: discharge voltage of the first discharge, T_1: discharge development time of the first discharge). Then, the discharge between shield and anode occurred (V_2: discharge voltage of the second discharge, T_2: discharge development time of the second discharge), resulting in the whole discharge through cathode-shield-anode (c-s-a). Due to the cathode and the shield were shorted by the first discharge, the shield potential V_s jumped up to the applied voltage V_a. The discharge via shield was discriminated and confirmed by the light emission.
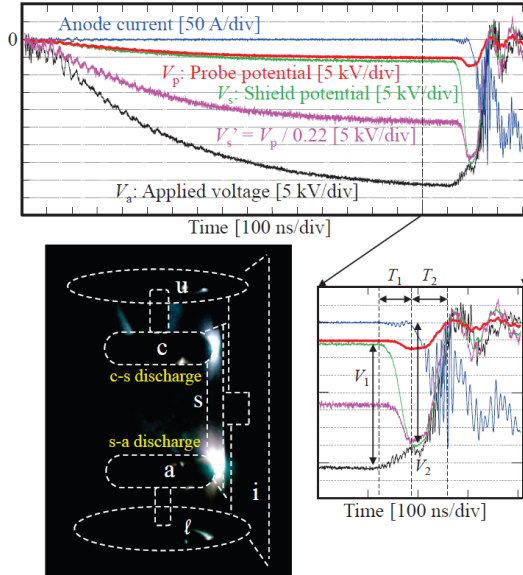
Before the discharge, as shown in Figure 6, the ratio

Figure 5. Discharge waveforms and light emission for c-s-a discharge ($V_a = -43$ kV$_{peak}$).
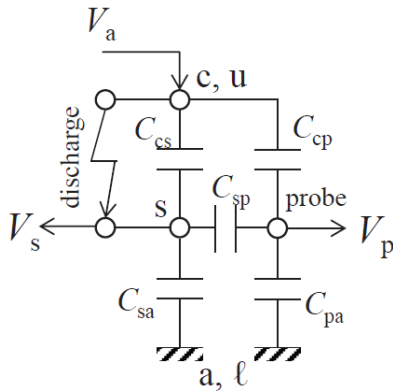

Figure 6. Equivalent circuit to calculate V_p / V_s.

between the probe potential V_p and the shield potential V_s was determined by the capacitance distribution between the electrode gaps as follows:

$$\frac{V_p}{V_a} = \frac{C_{cs}C_{sp} + C_{cp}(C_{cs} + C_{sp} + C_{sa})}{C_{sp}(C_{cs} + C_{sa}) + (C_{cp} + C_{pa})(C_{cs} + C_{sp} + C_{sa})} \cdots (1)$$

$$\frac{V_s}{V_a} = \frac{C_{cp}C_{sp} + C_{cs}(C_{cp} + C_{sp} + C_{pa})}{C_{sp}(C_{cp} + C_{pa}) + (C_{cs} + C_{sa})(C_{cp} + C_{sp} + C_{pa})} \cdots (2)$$

where C_{cp} is capacitance between cathode and probe, C_{pa} is capacitance between probe and anode, C_{cs} is capacitance between cathode and shield, C_{sa} is capacitance between shield and anode, C_{sp} is capacitance between shield and probe. The capacitances were measured by LCR meter. According to equations (1) and (2), V_p/V_s=94% before the discharge was calculated and verified in Figure 5.

After the first discharge between cathode and shield, V_p/V_s was determined by a new capacitance distribution between the electrode gaps, because the cathode and the shield were shorted, as follows:

$$\frac{V_p}{V_s} = \frac{C_{cp} + C_{sp}}{C_{cp} + C_{sp} + C_{pa}} \cdots\cdots\cdots (3)$$

According to equation (3), V_p/V_s=22% after the first discharge was calculated and verified in Figure 5.

Therefore, the relation between V_p and V_s is clear in the discharge process. Conversely, we can determine the shield potential from the equation $V_s' = V_p/22\%$ so as to discriminate the discharge pattern, even if we cannot measure the shield potential directly.

3.3 VERIFICATION TESTS

In order to confirm the effectiveness of the discharge pattern discrimination method with an electrostatic probe, we executed iterative verification tests based on the discrimination flowchart in Figure 2. As shown in Table 1, the tests results revealed that the discrimination success rate with an electrostatic probe was almost the same as that by direct measurement of the shield potential. The details of discrimination process for c-s-a discharge pattern are shown as follows:

Table 1. Verification tests results

Discharge pattern	c-s	c-s-a	u-i-s-i-ℓ	c-s-i-ℓ	not available	Total
Discharge site in VI Model					—	—
Frequency (by shield)	2	6	3	1	2	14
Frequency (by probe)	2	6	3	0	3	14

STEP 1:

Firstly, in Figure 5, we focus on the waveform V_s' that was calculated from V_p ($V_s' = V_p/22\%$, according to previous section). Because the calculated shield potential V_s' jumped up to the instantaneous cathode voltage and fell down to 0 V together with the cathode voltage, it can be determined that the discharge passed through the shield and short-circuited between the cathode and the anode. Such a two-step change in discharge waveforms means that this discharge pattern has two processes, we call them the first process and the second
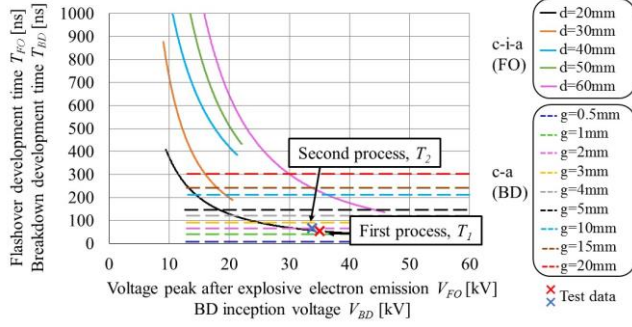

Figure 7. Discharge development characteristics for c-s-a pattern ($V_a = -43$ kV$_{peak}$).
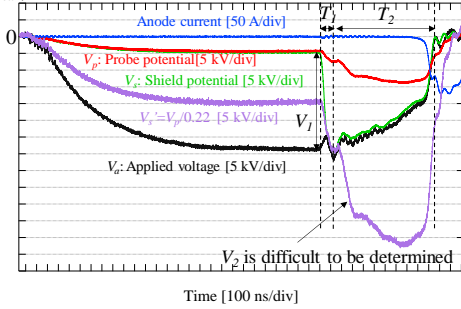

Figure 8. Discharge waveforms and light emission for c-s-i-ℓ discharge ($V_a = -34$ kV$_{peak}$).

process, respectively.

STEP 2:

For the first process in Figure 5, the discharge development time T_1 was 60 ns and the discharge voltage V_1 was 35 kV. For the second process, the discharge development time T_2 was 70 ns and the discharge voltage V_2 was 33 kV. The sets of (V_1, T_1) and (V_2, T_2) were plotted in Figure 3, as shown in Figure 7. T_1 is consistent with the BD development time in about 1 mm gap,

and also consistent with the FO development time in the creepage distance of about 20 mm.

STEP 3:

By the consideration of the internal structure and dimension of the VI model in Figure 4, the first process can be identified as discharge between the cathode and the shield (c-s). The relationship between V_2 and T_2 was also consistent with BD in 1 mm gap and FO in 20 mm creepage distance. The same reason as the first process, the second process can be determined as BD between the shield and the anode (s-a) with 1 mm gap. From the light emission of discharge in Figure 5, we confirmed that the discharge occurred at c-s and s-a, i.e. c-s-a, which is consistent with the above discrimination result.

In some cases, such as c-s-i-ℓ pattern near the electrostatic probe in Figure 8, due to the influence of flashover channel potential, the shield potential was not determined by the capacity distribution between the electrode gaps. Therefore, it was difficult to evaluate V_2 and resulted in the discrimination failure. However, this problem can be solved by using an array of electrostatic probes on the insulator surface of VI, as shown in Figure 9, where some probes would detect the shield potential, irrespective of the internal flashover path. It is also expected to discriminate and identify the flashover path, which might be better than the direct measurement of shield potential. For the application of this technique to an actual vacuum interrupter, the size and position of the electrostatic probe may affect the accuracy of shield potential measurement, as estimated by equations (1)-(3), due to the change of the capacitances distribution of electrode gaps. Therefore, the size and position of the electrostatic probe should be checked carefully.
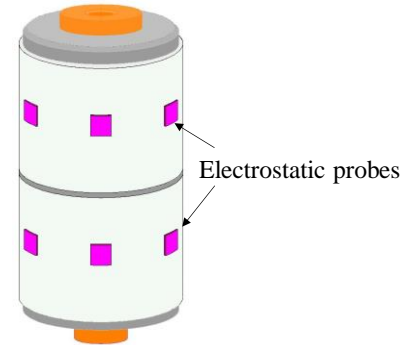

Figure 9. Prospective arrangement of electrostatic probes on the insulator surface of VI.

4 CONCLUSION

In order to discriminate the discharge pattern in vacuum interrupters, based on the discharge development characteristics, we proposed a novel discrimination method of the discharge pattern in vacuum. In this discrimination method, the measurement of electrical parameters (applied voltage, anode current, shield potential) is necessary. For the case that the shield potential cannot be measured directly, we developed

a new non-contact measurement method of the shield potential with an electrostatic probe. Furthermore, verification tests using this measurement method were conducted and the effectiveness of the discrimination method was verified. This work will contribute to the identification of the insulation weak points in vacuum interrupters as well as to the advanced and reliable insulation design of vacuum circuit breakers.

REFERENCES

[1] Paul G. Slade: "The vacuum interrupter: Theory, Design, and Application", CRC press, pp.1-6, 2007.

[2] H. Okubo, H. Kojima, K. Kato, N. Hayakawa and M. Hanai, "Advanced Electrical Insulation Techniques for Higher Voltage Vacuum Interrupters", CIGRE B3/D1 Colloquium, No.218 (2013).

[3] L. T. Falkingham, "Vacuum Interrupter Design for HV and VHV Applications", the 22nd Int'l. Sympos. Discharges and Electr. Insulation in Vacuum, pp.204-207, 2006.

[4] F. Kong, H. Kojima, M. Tsukima, T. Kimura, and N. Hayakawa: "Discharge Pattern Discrimination for Composite Insulation System in Vacuum interrupter", XXVIIth Int. Symp. on Discharges and Electrical Insulation in Vacuum, Sep.18-23, 2016

[5] F. Kong, H. Kojima, T. Kimura, M. Tsukima, and N. Hayakawa,: "Discharge Pattern Discrimination for Composite Insulation System in Vacuum", IEEJ Transactions on Fundamentals and Materials, Vol.136, No.9, pp.594-602 (2016) (in Japanese)

[6] Gennady A. Mesyats and D.I. Proskurovsky, Pulsed Electrical Discharge in Vacuum, 1st ed., Springer-Verlag, pp.118-135, 1989.

[7] E. Hantzsche, "Theory of the Expanding Plasma of Vacuum Arcs", J. Phys. D: Appl. Phys., Vol. 24, pp. 1339-1353, 1991.

[8] I. I. Beilis, "State of the Theory of Vacuum Arcs", IEEE Trans. Plasma Sci., Vol. 29, No. 5, pp. 657-670, 2001.

[9] F. Kong, Y. Nakano, H. Kojima, N. Hayakawa, T. Kimura, and M. Tsukima: "Discharge Characteristics for Various Discharge Patterns under Negative Lightning Impulse Voltage in Vacuum", IEEE Transactions on Dielectrics and Electrical Insulation, Vol. 23, No.2, pp. 813-818 (2016)

[10] F. Kong, Y. Nakano, H. Kojima, N. Hayakawa, T. Kimura, and M. Tsukima: "Discharge Characteristics of Composite Insulation System with Floating Electrode and Solid Insulator in Vacuum", IEEE Transactions on Dielectrics and Electrical Insulation, Vol. 23, No.2, pp. 1219-1225 (2016)

[11] R. A. Anderson and J. P. Brainard, "Mechanism of Pulsed Surface Flashover Involving Electron-stimulated Desorption", J. Appl. Phys., Vol. 51, No. 3, pp. 1414-1421, 1980.

[12] A. S. Pillai and R. Hackam, "Surface Flashover of Solid Dielectric in Vacuum", J. Appl. Phys., Vol. 53, No. 4, pp. 2983-2987, 1982.

[13] A. A. Neuber, M. Butcher, H. Krompholz, L. L. Hatfield and M. Kristiansen, "The Role of Outgassing in Surface Flashover under Vacuum", IEEE Trans. Plasma Sci., Vol. 28, No. 5, pp. 1593-1598, 2000.

Fei Kong (S'14−M'16) was born on 13 July in 1987. He received the M.S. degree in electrical engineering from Beijing Jiaotong University, Beijing, China, in 2011. He received the Ph.D. in 2016 in Electrical Engineering and Computer Science from Nagoya University (MEXT scholarship), Japan. His major research interests include discharge phenomena and electrical insulation in vacuum. Dr. Kong is a member of IEE of Japan.

Hiroki Kojima (M'11) was born on 7 December 1975. He received the Ph.D. degree in 2004 in energy engineering and science from Nagoya University. Since 2004, he has been at Nagoya University and presently he is an Associate Professor of Nagoya University at the Department of Electrical Engineering and Computer Science. Dr. Kojima is a member of IEE of Japan.

Naoki Hayakawa (M'90) was born on 9 September 1962. He received the Ph.D. degree in 1991 in electrical engineering from Nagoya University. Since 1990, he has been at Nagoya University and presently he is a Professor of Nagoya University at the Department of Electrical Engineering and Computer Science. From 2001 to 2002, he was a guest scientist at the Forschungszentrum Karlsruhe/Germany. Prof. Hayakawa is a member of CIGRE and IEE of Japan.

Toshinori Kimura was born in Japan on 27 June 1964. He received the B.S. and M.S. degrees in physics from Hokkaido University in 1988 and 1990, respectively. In 1990, he joined Mitsubishi Electric Corporation. Presently, he is engaged in researching

arc physics and the development of vacuum circuit breakers in Advanced Technology R&D Center. Mr. Kimura is a member of IEE of Japan.

Mitsuru Tsukima was born in Kyoto, Japan, on 2 June 1970. He received the B.S. and M.S. degrees in applied physics from Osaka University, Osaka, Japan, in 1994 and 1996, respectively. He joined the Advanced Technology R&D Center, Mitsubishi Electric Corporation, Amagasaki, Japan, in 1996. He is currently working on circuit breakers and related technologies. Dr. Tsukima is a member of IEE of Japan.